ELECTRONICS AND ELECTRICAL ENGINEERING
ISSN 1392 – 1215 2012. No. 1(117)
ELEKTRONIKA IR ELEKTROTECHNIKA

HIGH FREQUENCY TECHNOLOGY, MICROWAVES
T 191
AUKŠTŲJŲ DAŽNIŲ TECHNOLOGIJA, MIKROBANGOS

Radiation Pattern Analysis and Advanced Phase Shifter Development for designing Phased Smart Antenna Arrays

O. M. Manu, M. Dimian, A. Graur
Dept. of Electrical Engineering and Computer Science, Stefan cel Mare University of Suceava, Str. Universitatii nr. 13, Suceava, Romania, phone: +40230216147 int. 229, e-mails: octavianm@eed.usv.ro, dimian@eed.usv.ro, adrian.graur@usv.ro

crossref http://dx.doi.org/10.5755/j01.eee.117.1.1063

Introduction

Smart Antennas systems have received an increasing amount of research interest over the last years due to the great potential for applications in telecommunications and defense industry [1–3]. In the area of localization and scanning applications, the non-inertial beamforming and beam scanning of the smart antenna allows very fast beam switching and target identification, as well as simultaneous monitoring of multiple targets which is not possible using traditional inertial systems. Smart antennas also reduce the influence of multipath effects on the estimation of target location in indoor localization systems [4].

A special interest in the area of telecommunications is devoted to optimizing the use of wireless communication channels [5]. The higher antenna gain of the antenna arrays increases the signal to noise ratio, and consequently, decreases the bit error rate over the communication channel. Other optimizations brought by smart antennas in the field of communication systems include the increasing of the spectral efficiency, the reducing of the transmitted power, of the co-channel interference, and of the multipath interferences. Smart antennas can also monitor and track mobile users, allowing and improvement of both signal range and the quality of service [6, 7].

Novel developments [8] in the area of wireless smart sensor network (WSN) could also benefit from using Smart Antennas in applications like monitoring an environment in dangerous regions, monitoring industrial or location applications. Beamforming in smart antennas is usually done by using high-performance computing algorithms which use both phase shift and amplitude variation of signals fed to antenna elements. Since WSN are mainly low power, battery operated devices, with low processing power capabilities there is a clear need to develop specific beamforming methods and algorithms featuring low computational cost. The solution developed in [9] by using the amplitude variance of the antenna array elements is relatively easy to implement but it does not provide a large scanning angle.

This article is focused on phase shift variation of signal feeding antenna elements, providing numerical simulations for the analysis and design of antenna characteristics and presenting the development of an advanced phase shifter implementation based on vector modulators used to implement the optimal solution.

Analytical Array Characteristics

In this section an analytical overview of various phased only antenna array with different geometries and number of elements The main beam of the antenna array must be narrow enough to allow the use of smart antenna in systems for position estimation and scanning based on a triangulation technique for determining the angle of arrival. These analytical considerations do not take into account the mutual coupling between antenna elements, which will be addressed by numerical means in section 3.

Let us consider an antenna array with N linear elements oriented along z-axis (see Fig. 1) with a linear phase difference between antenna elements of ψ_i. The total signal received by the antenna array in the horizontal plane at angle φ with y-axis can be written as follows [10]

$$S_a(\varphi) = S_e(\varphi)\sum_{i=1}^{N} e^{j[k_0(N-i)d\cdot\sin(\varphi)+\psi_i]}, \quad (1)$$

where $S_e(\varphi)$ represents the complex radiation pattern of one individual radiator, k_0 represents the free space wavenumber and d is the spacing between antenna elements. In order to form a beam in the desired direction φ_0, let us choose a linear phase taper of the following form

$$\psi_i = -k_0(N-i)d\sin(\varphi_0), \text{ for } i = 1,2,...,N. \quad (2)$$

The maximum of the corresponding array factor is attained for: $\sin(\varphi) - \sin(\varphi_0) = 0$, or, provided that

$-90° \le \varphi, \varphi_0 \le 90°$, for $\varphi = \varphi_0$. Thus, by choosing a desired beam-pointing direction φ_0 and subsequently phasing the linear antenna array elements according to (2), the array factor will reach its maximum at the desired angle $\varphi = \varphi_0$.

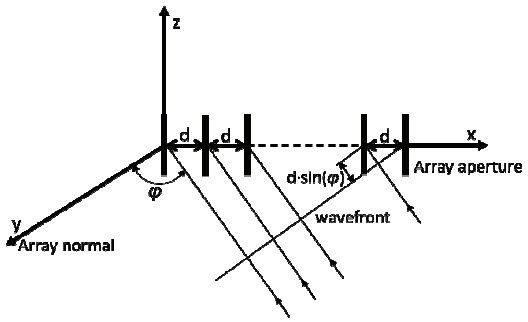

Fig. 1. Schematic representation of a linear antenna array

It is known [10] that the dependence of the main lobe beamwidth $\widetilde{\varphi}$ on the number of linear array elements can be approximated by the following relation

$$\widetilde{\varphi} = 0.8858\lambda / Nd\cos(\varphi_0)\,. \tag{3}$$

Next, let us consider a planar antenna array with K x L elements arranged in a rectangular lattice, grouped in a configuration of K rows, having an inter-element distance d_y between the rows and L columns with an inter-elements distance d_x between columns as shown in Fig. 2. This setup can be regarded for example as a linear antenna array directed along the x-axis, having linear arrays as elements, directed along the y-axis. The natural occurring phase difference ψ_{kl} of element (k,l) relative to the element (1,1) used as reference, is given by

$$\psi_{kl} = k_0(k-1)d_x\sin(\theta)\cos(\varphi) + k_0(l-1)d_y\sin(\theta)\sin(\varphi)\,, \tag{4}$$

where d_x and d_y represent the spacing between elements across X and Y axis, respectively.

The resulting planar array radiation pattern $S(\theta,\varphi)$ is given by the following formula

$$S(\theta,\varphi) = S_e(\theta,\varphi)\sum_{k=1}^{K}\sum_{l=1}^{L} e^{j(\psi_{kl}+\psi'_{kl})}\,, \tag{5}$$

where $S_e(\theta,\varphi)$ represents the element radiation pattern.

In order to steer the beam in the desired a phase taper that satisfies the following relation must be chosen

$$\psi'_{kl} = -k_0(k-1)d_x\sin(\theta_0)\cos(\varphi_0) - k_0(l-1)d_y\sin(\theta_0)\sin(\varphi_0)\,, \tag{6}$$

where (θ_0,φ_0) indicates the direction for the desired beam.

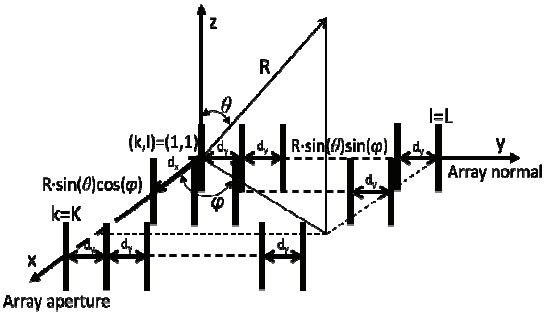

Fig. 2. Schematic representation of a planar antenna array

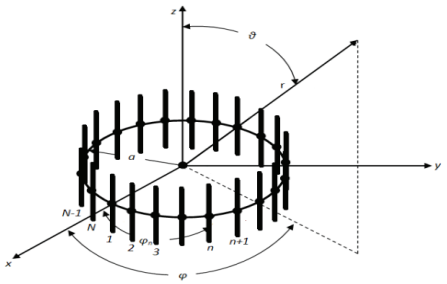

Fig. 3. Schematic representation of a circular antenna array

Since the array is made of dipole radiators which in the xy plane have isotropic radiation pattern, the array factor becomes the antenna radiation pattern. It is apparent from this expression of the array factor that the maximum of the array radiation will occur for $(\theta, \varphi) = (\theta_0, \varphi_0)$.

Let us now consider a circular antenna array with N elements arranged in a circular configuration of radius a as shown in Fig. 3 [11]. The resulting circular array radiation pattern $S(\theta,\varphi)$ is given by the following formula

$$S(\theta,\varphi) = S_e(\theta,\varphi)\sum_{n=1}^{N} e^{j(\psi_n + a_n)}\,, \tag{7}$$

where $S_e(\theta,\varphi)$ represents one element radiation pattern and ψ_n the natural occurring phase difference of element n relative to the first element used as reference and is given by

$$\psi_n = k_0 a\sin(\theta)\cos(\varphi - 2\pi(n/N))\,. \tag{8}$$

In order to steer the beam in the desired direction (θ_0,φ_0), we must apply a progressive phase shifts between array elements that satisfies the following relation

$$a_n = -k_0 a\sin(\theta_0)\cos(\varphi_0 - 2\pi(n/N))\,. \tag{9}$$

Next, the influence of mutual coupling between antenna elements on the array radiation patterns will be addressed by numerical means.

Antenna array simulations

In the case of applications involving the estimation of direction of arrival, the optimum antenna array configuration is the one with the inter element spacing equal to the half wavelength. Antenna array simulations were performed by using 4NEC2 software which computes the numerical solution of integral equations for induced currents and simulates the electromagnetic response of antennas and metallic structures by using Method of Moments. By solving the impedance matrix the 4NEC2 software takes into account the mutual coupling between antenna elements. The software computes successively the currents on the antenna components for each excitation source of the array elements. Those currents are used to compute the array impedance matrix, and all embedded element patterns. Antenna array elements used in the simulations are half wavelength dipoles which provide an omnidirectional radiation pattern in the plane perpendicular to the dipoles. A large number of numerical simulations have been performed for various geometrical configurations of antenna arrays and different phase shift

applied between antenna elements according to Eqs. (2), (6) and (9) and the results were compared to the corresponding analytical calculations based on Eqs. (1), (5) and (7). 3D radiation pattern of 12 elements linear and circular antenna and of 16 elements planar array are presented in Fig. 4(a), Fig 5(a) and in Fig. 6(a).

The analysis performed over the linear antenna array shows, as expected, that increasing the number of array elements the half power beamwidth (HPB) of the major lobes in the horizontal plane is decreasing for each scanning angle.

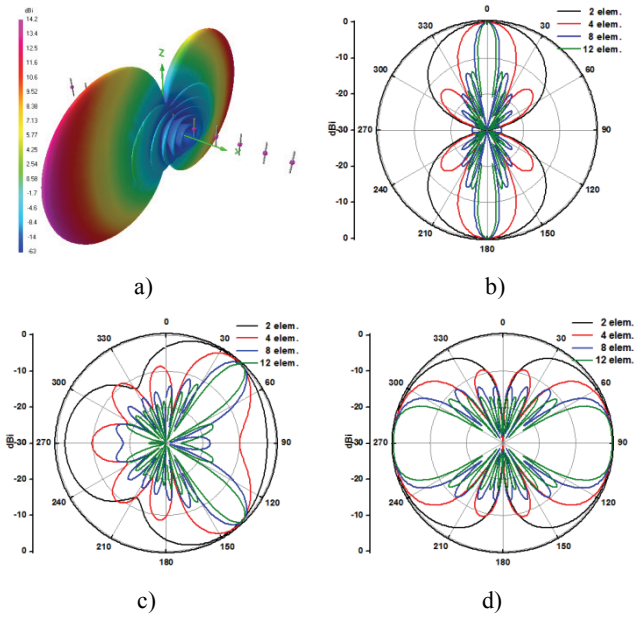

Fig. 4. 3D radiation pattern of 12-elements linear antenna array with $\varphi_0 = 0°$(a) and cross-sections of various linear antenna arrays with $\varphi_0 = 0°$(b), $\varphi_0 = 45°$(c) and $\varphi_0 = 90°$(d)

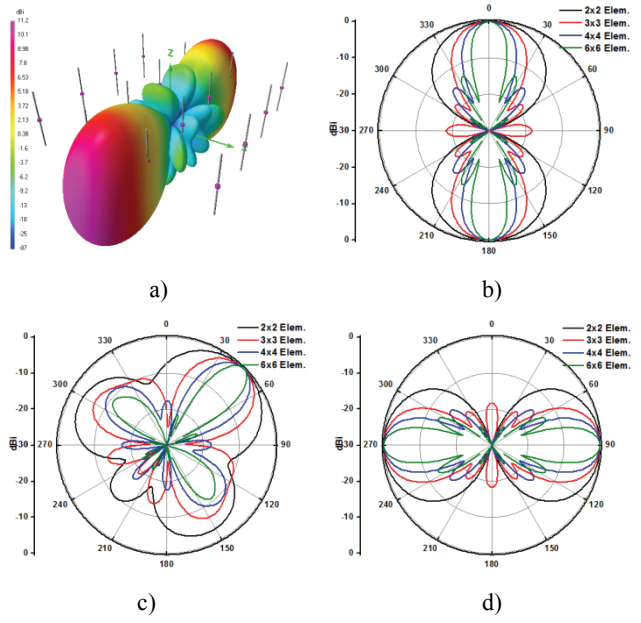

Fig. 5. 3D radiation pattern of 16-elements planar antenna array with $\varphi_0 = 0°$(a) and cross-sections of various planar antenna arrays with $\varphi_0 = 0°$(b), $\varphi_0 = 45°$(c) and $\varphi_0 = 90°$(d)

In Fig. 4(b),(c) and (d) the variation of HPB of arrays with 2, 4, 8 and 12 elements, at a scanning angle of 0°, 45° and 90° it is visible. A slightly less decrease of the HPB with the increase in the number of array elements is observed on planar antenna arrays with configurations of 2x2, 3x3, 4x4 and 6x6 elements, at scanning angles of 0°, 45° and 90°, as seen in Fig. 5(b),(c) and (d). In circular antenna array configurations the effect of the decreasing of the HPB is the smallest among the antenna arrays analyzed as seen on Fig. 6(b),(c) and (d) for configurations of 8, 12, 16 and 18 elements at scanning angles of 0°, 45° and 90°.
It has been observed for all geometrical configurations that the half power beamwidth (HPB) of the major lobes in the horizontal plane is decreasing with the increase in the

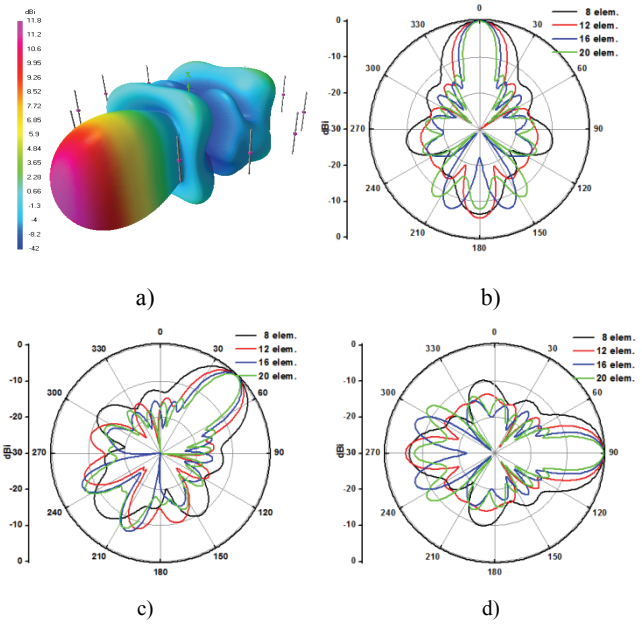

Fig. 6. 3D radiation pattern of 12-elements circular antenna array with $\varphi_0 = 0°$(a) and cross-sections of various circular antenna arrays with $\varphi_0 = 0°$(b), $\varphi_0 = 45°$(c) and $\varphi_0 = 90°$(d)

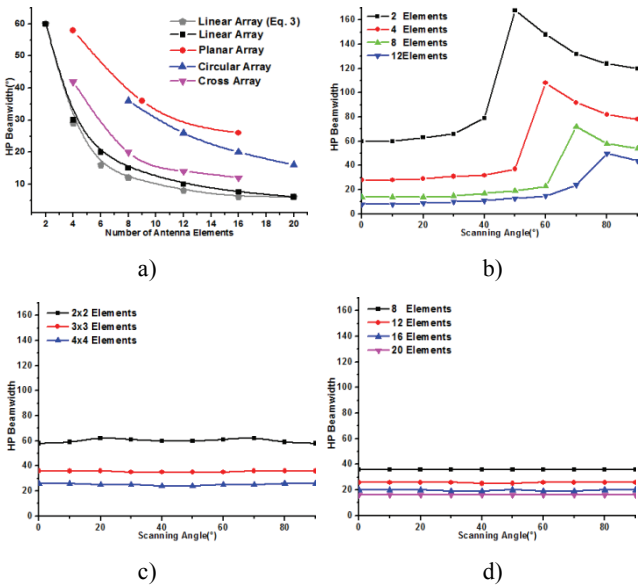

Fig. 7. HPB vs. the number of elements for various array configurations (a); HPB vs. scanning angle for different linear array (b), planar array (c) and circular array (d)

number of elements as shown in Fig. 7(a).

Although linear phased antenna arrays have a better performance in the horizontal plane, circular phased antenna arrays provide a better characteristic when 3D analysis is considered. In addition, the horizontal HPB of main lobes is widening with the increase of scanning angle for linear arrays as seen in Fig. 7(b), while they remains almost constant for planar and circular configurations, as seen in Figs. 7(c) and (d).

It can be also proven that mutual coupling have an important influence on other antenna arrays characteristics.

Hardware implementation

The theoretical analysis summarized in the previous section suggested that a 12 elements linear antenna array provide the best solution for implementing a low cost and low power smart antenna for Radio Frequency Identification or Wireless Sensor Networks in the case of horizontal scanning, while a 16 elements circular antenna array would be best suited for the case of 3d scanning. In order to implement these solutions, the main step is to develop an advanced phase shifters. Various solutions are used for implementing phase shifters, such as delay lines [12-13]. A phase shifter system based on the vector modulator integrated circuit AD8340 provided by Analog Devices was designed. A picture of the developed phase shifter is provided in Fig. 8.

The vector modulator via an integrated polyphase network splits up the input signal in an in-phase (I) and a quadrature (Q) component. These signals are then feed to separate balanced linear variable attenuators for I and Q channel which independently scale I and Q components of the RF input. The attenuators outputs are summed to the output of the circuit. These internal balanced attenuators allow changings of the corresponding channel polarity, thus a true 0° to 360° phase shift can be obtained. The maximum attenuation range of the input signal is 30 dB. The phase shifter is controlled by an 8 bit RISC microcontroller via 16 bit digital to analog converters. The microcontroller receives phase and attenuation values from a PC via USB interface, computes the digital values for the Digital to Analog Converters and then sends these data over a SPI interface to the corresponding DAC. The entire hardware setup was made on low cost dual layer RF-4 laminate with a dielectric height of 1.5mm, a relative permittivity of 4.5 and a loss tangent of $15 \cdot 10^{-3}$ at a frequency of 1GHz.

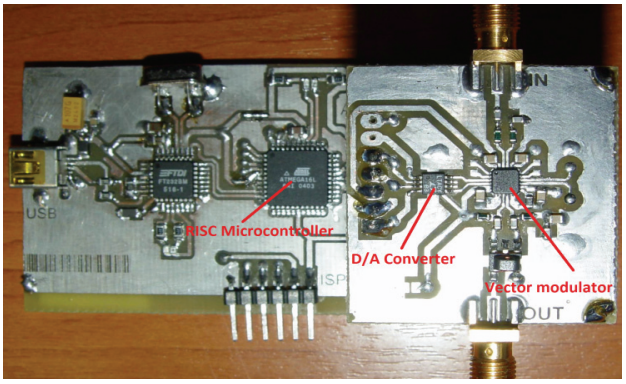

Fig. 8. Phase shifter based on vector modulator

The characteristics of the phaseshifter circuit were measured with a Vector Network Analyzer. The S11 reflection coefficient and S21 transmission parameter were measured both in magnitude and phase between 700MHz and 1GHz, covering the entire frequency band of the AD8340 vector modulator. The measurements were conducted for phase setpoints between 0 and 360 degrees and for attenuation values between 0% corresponding to no additional induced attenuation and 75%. The maximum value of 100% corresponds to a 30dB attenuation of the signal passing through the phaseshifter.

In Fig. 9 the magnitude values of S11 parameters were plotted for 4 different attenuations of 0%, 25%, 50% and 75%. As it can be observed from Fig. 9 the reflection coefficient maintains a value below -17dB for entire frequency range with a minimum of approximately -37dB around 760MHz. In Fig. 10 the S11 magnitude error of attenuation values of 25%, 50% and 75% relative to 0% attenuation were plotted. It is visible that changes of the attenuation values have a very low impact on the values of reflection coefficient, with errors below 2.5%.

The magnitude and phase of S21 transmission coefficients for our phaseshifter were recorded for phase setpoints between 0 and 360 degree with a phase step of 1 degree at the attenuations values of 0%, 25%, 50% and 75% for 866.5MHz driving frequency.

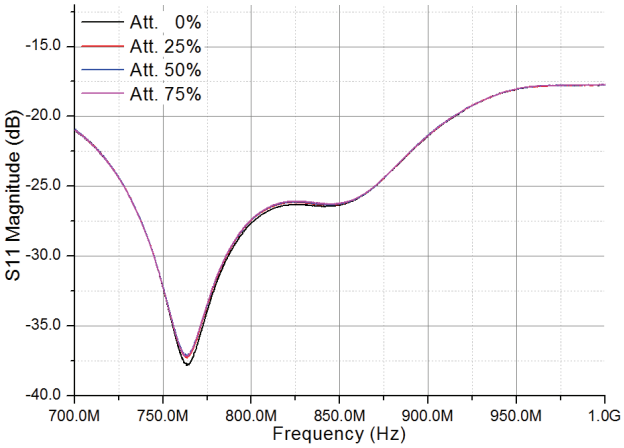

Fig. 9. Variations with the frequency of the S11 Magnitude for the phaseshifter at various attenuation values

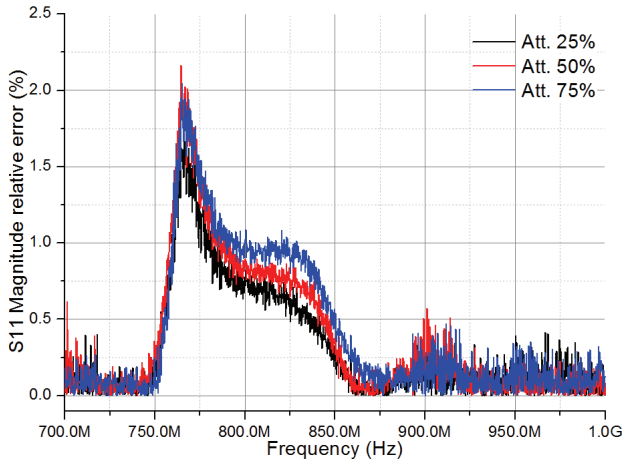

Fig. 10. S11 Magnitude relative error between different attenuation values

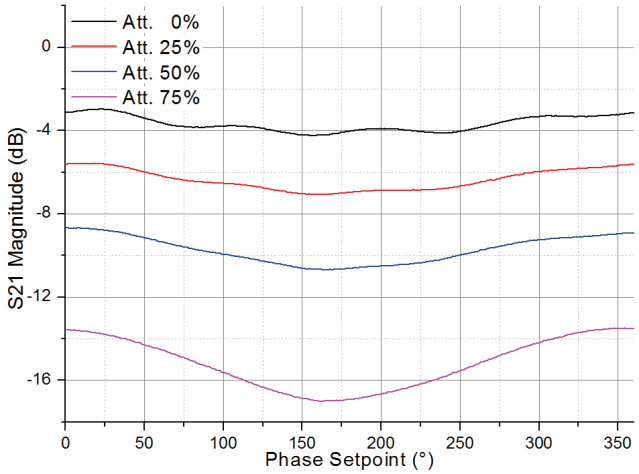

Fig. 11. S21 magnitude values of phaseshifter at various phase setpoint with different attenuation values

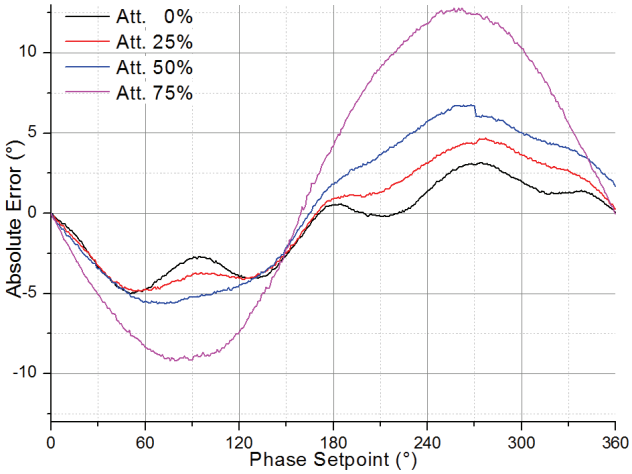

Fig. 13. S22 absolute phase error of phaseshifter at various phase setpoint and attenuations

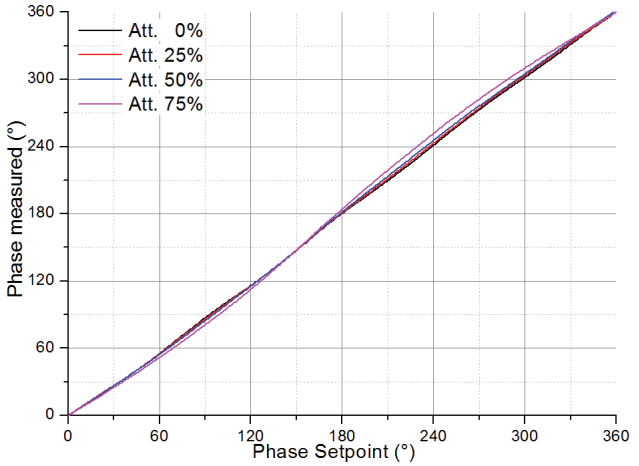

Fig. 12. S22 phase values of phaseshifter at various phase setpoint and attenuations

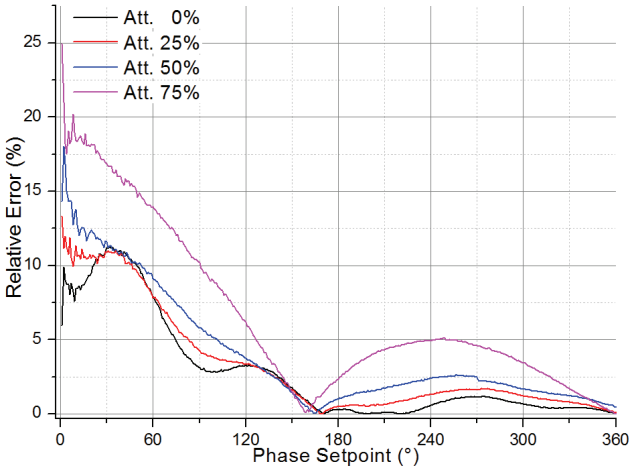

Fig. 14. S22 phase error of phaseshifter at various phase setpoint and attenuations relative to phase setpoint

The 866.5MHz represent the middle point of the 865-868MHZ allocated frequency band for RFID applications in European Union [14]. Fig. 11 presents the magnitude of the S21 parameter at various phase setpoint and attenuation. It is visible that for low values of attenuation the S21 magnitude is relative constant with variations below 1dB for the entire range of 360 degree. As the attenuation increases the S21 magnitude has an increased variation of up to 3dB for 75% attenuation.

The Fig. 12 presents the phase of the S22 parameter for various attenuation level and phase setpoints between 0 and 360 degree with 1 degree step. The phase shift induced by the advanced phaseshifter is linear with the phase setpoint, having for 0% attenuation an absolute phase error between -5 and +3 degree as seen from Fig. 13. With the increase of attenuation, the absolute phase error values increases to -9 to +13 degree for 75% attenuation value. Fig. 14 presents the relative error of expected S21 phase coefficient for various attenuation values and a phase setpoint sweep between 0 and 360 degree. As already noted the relative error has the smaller values of 10% or less for 0% attenuation. As the attenuation raises to 75% the relative error increases to 20%-25% for phase setpoint bellow 10° and to 5% for phase setpoint above 120°.

The implementation of linear and circular antenna arrays using this phase shifter is currently under development in our laboratory. Preliminary measurements of radiations pat-terns for 2 and 4-elements phased antenna array based on the developed phase shifter have been performed in the TDK semi-anechoic chamber of our laboratory and have been proven to be in good agreement with the numerical simulations presented above.

Conclusions

The use of smart antenna applications in consumer electronics is rather limited due to the relatively high cost, complexity and power consumption of the existent implementations. This article has presented an analysis of various antenna array configurations for beamforming by using phase taper only as well as a hardware implementation of an advanced phase shifter based on a vector modulator integrated circuit. The HPB of the major lobes decreases with the increase of array elements in each array geometry. However, a special attention should be paid to the side lobes whose number increases as antenna become larger. In linear antenna array special attention must be paid to endfire scenario where the HPB of the

major lob increases significantly. The main beams of planar and circular arrays are not affected as much by changing the scanning angle. However for scanning angles less than 40° the linear array offers the smallest HPB for same element number.

This analysis suggest the choose of a 12 elements linear antenna array for implementing a low cost and low power smart antenna in the case of horizontal scanning, and a 16 elements circular antenna array for the case of 3d scanning. The hardware implementation included the development of an advanced phase shifter that proved good phase shift accuracy and stability in the frequency region of interest. The advanced phaseshifter provides a linear phase shift with relative errors under 12% for phase setpoint between 0 and 80° and fewer than 5% for the rest. Also the attenuation was relative constant for small imposed attenuation values. As the imposed attenuation increases the phase errors and attenuation nonlinearity increase to some level and corrections must be taken into account when developing smart antenna using phase shifters base on vector modulator.

Acknowledgements

This work was supported partially by E.U. funds, under the contract no. POSDRU/6/1.5/S/22 and by E.U. Framework Program 7 under contract no. PIRG02-GA-2007-224904.

References

1. **Dyadyuk V., Guo Y.J.** Towards multi–gigabit ad–hoc wireless networks in the E–band // Global Symp. on Millimeter Waves, 2009.
2. **Simons J., Ivashina M., et al.** Beamformer system model of focal plane arrays in deep dish radio telescopes // European Radar Conf. (EURAD'2005), 2005. – P. 355–358.
3. **Fabrizio G., Colone F., Lombardo P., et al.** Adaptive beamforming for high–frequency over–the–horizon passive radar // IET Radar Sonar Navig., 2009. – Vol. 3. – P. 384–405.
4. **Buta G., Coca E., Graur A.** Path Loss Exponent Influence on Distance Estimation between Wireless Sensor Nodes // Advances in Electrical and Computer Engineering, 2010. – Vol. 10. – No. 1. – P. 110–115
5. **Potorac A. D., Onofrei A., Balan A.** An Efficiency Optimization Model for 802.11 Wireless Communication Channels // Electronics and Electrical Engineering. – Kaunas: Technologija, 2010. – No. 1(97). – P. 67–72
6. **Liu H., Darabi H., Banerjee P., et al.** Survey of Wireless Indoor Positioning Techniques and Systems // IEEE Transactions on Systems, Man, and Cybernetics, Part C: Applications and Reviews, 2007. – Vol. 37. – No. 6. – P. 1067–1080.
7. **Abdulmonem T. M., Elsohby A., Hossam B., Shokry A., Eshrah I. A.** Adaptive Antenna for Wi–Fi System Enhancement // Potentials. – IEEE, 2011. – Vol. 30. – Iss. 1. – P. 30–34.
8. **Paradells J., Vilaseca J., Casademont J.** Improving security applications using indoor location systems on wireless sensor networks // Proc. of the International Conference on Advances in Computing, Communication and Control, 2009. – P. 689–695.
9. **Sayidmarie K. H., Jasem B. J. M.** Amplitude–only beam scanning in linear antenna arrays // Proc. of the International Multi–Conference on Systems Signals and Devices (SSD), 2010.
10. **Hansen C. R.** Phased Array Antennas. – John Wiley & Sons, 2009. http://dx.doi.org/10.1002/9780470529188.
11. **Volakis J.** Antenna Engineering Handbook. – McGraw–Hill, 2007.
12. **Urbanavičius V., Gurskas A., Martavičius R.** Simulation of the Meander Delay Line using the Hybrid Method // Electronics and Electrical Engineering. – Kaunas: Technologija, 2009. – No. 2(90). –P. 1–6
13. **Gurskas A., Urbanavičius V., Martavičius R.** Evaluation of the Microstrip Lines Connectors in the Meander Delay Line Model // Electronics and Electrical Engineering. – Kaunas: Technologija, 2010. – No. 3(99). – P. 39–43.
14. **Turcu C. (ed.)** Radio Frequency Identification Fundamentals and Applications, Bringing Research to Practice. – Intech, 2010.

Received 2011 04 05
Accepted after revision 2011 06 23

O. M. Manu, M. Dimian, A. Graur. Radiation Pattern Analysis and Advanced Phase Shifter Development for designing Phased Smart Antenna Arrays // Electronics and Electrical Engineering. – Kaunas: Technologija, 2012. – No. 1(117). – P. 105–110.

This paper presents an analysis of beamforming and radiation pattern of various phased antenna arrays configurations which are intended for use in low cost Radio Frequency Identification or Wireless Sensor Networks applications for wireless process monitoring and location. The location process is based on the estimation of direction-of-arrival by determining the angle-of-arrival of radio signals. The beamforming and the steering of the antenna's lobes are obtained via a linear phase excitation of the signal applied to the array elements. Several configurations of various geometries and sizes are analyzed in order to obtain an array with narrow main beam and good scanning capabilities. Finally, the main elements of the developed hardware implementation involving phase shifter based on vector modulators are discussed. Ill. 14, bibl. 14 (in English; abstracts in English and Lithuanian).

O. M. Manu, M. Dimian, A. Graur. Kryptingumo diagramų analizė ir fazės sukiklio sukūrimas projektuojant fazuotų išmaniųjų antenų masyvus // Elektronika ir elektrotechnika. – Kaunas: Technologija, 2012. – Nr. 1(117). – P. 105–110.

Pateiktos įvairių fazuotų antenų masyvų, skirtų naudoti pigiose radijo dažnio identifikavimo arba bevielių jutiklių tinklų sistemose, konfigūracijų kryptingumo diagramos. Lokacijos procesas pagrįstas krypties nustatymu įvertinant radijo signalų sklidimo kampą. Spindulys formuojamas ir antenos dalys reguliuojamos žadinant signalo, siunčiamo į masyvo elementus, fazę. Ištirtos kelios įvairių matmenų ir geometrijų konfigūracijos siekiant nustatyti masyvą su siaura diagrama ir geromis skenavimo galimybėmis. Aptarti pagrindiniai aparatinės realizacijos elementai. Il. 14, bibl. 14 (anglų kalba; santraukos anglų ir lietuvių k.).